# Magnetic Field Dependent NV Center spin dynamics and ODMR Simulation

-

**Abstract**

The rapidly advancing domain of quantum sensing has emerged as a pivotal frontier in foundational and applied physics, with negatively charged nitrogen-vacancy (NV) centres leading the charge. This paper comprehensively reviews the spin dynamics of NV centres under the combination of a static and a perturbative magnetic field. We study the Optically Detected Magnetic Resonance (ODMR) of a single NV centre at depth. However, many implementations and simulations benefit from using large ensembles for increased signal output and sensitivity. Here, we extrapolate the theory for a single NV centre to the complete ensemble. We present a simulation tool created along the lines of the presented theory that computes and plots the ODMR contrast of the single and the ensemble.

*keywords: nitrogen - vacancy (NV) centres, Optically Detected Magnetic Resonance (ODMR), spin dynamics, contrast, noise*

## 1 Introduction

The nitrogen-vacancy (NV) centre in diamond, comprising a substitutional nitrogen atom adjacent to a lattice vacancy, has captured significant interest due to its exceptional capabilities like long coherence time and read-out by pure optical methods by using its photo-stable spin-dependent photoluminescence (PL). These capabilities have made NV defect a very promising candidate for quantum sensing and quantum information applications [3]. NV centres have been utilized in several other fields, including but not limited to quantum registers [1], quantum computing [2], time measurement [7], electric field measurement [4], rotation sensing[13], and nuclear magnetic resonance applications [12].

It is possible to find NV centers in 3 possible charged states, $NV^0, NV^-, and NV^+$, however $NV^-$(From now on, it'll be referred as NV for simplicity) is most widely studied for quantum sensing and quantum information applications due to its favourable energy structure and photophysics [3]. The NV defect exhibits a triplet ground and excited state with three spin sublevels (ms=+1,0,-1) alond with two singlet intermediate states [3]. In the triplet ground state, $m_s$=+1 and $m_s$=-1 are degenerate, separated from the $m_s$=0 by Zero Field splitting Energy(Dgs).The degeneracy between $m_s$=+1 and $m_s$=-1, can be lifted by magnetic fields parallel to the NV axis due to the Zeeman shift. At room temperature, the electrons in the triplet ground state can be excited to the triplet state by green laser irradiation (532 nm). The excited state decays to the ground state via a radiative process with a zero-phonon line at 637 nm, accompanied by non-radiative transitions through the singlet states. The different decay rates for various spin projections during the non-radiative process result in optically initializing the system into the $m_s = 0$ state of the ground level. This decay mechanism also allows for spin state readout, as it produces different photoluminescence(PL) intensities for the $m_s = 0$ and $m_s$=$\pm$1 states. This spin dependent PL allows us to plot the graph of the optically detected magnetic resonance (ODMR).

In this study, we use the Continuous Wave ODMR method, though advanced pulsed techniques could improve magnetic field detection sensitivity. An ODMR spectrum of an NV ensemble can reveal detailed information, allowing reconstruction of the magnetic field vector around an NV center. We have simulated the ODMR spectra of an NV ensemble under an external magnetic field and a perturbative microwave field. We used transition rates and spin populations to calculate the contrast of the ODMR spectrum, applying Fermi's golden rule to account for Rabi oscillations induced by the microwave field . To test the robustness of our model, we introduced noise, including photon-shot noise and noise from other impurities in the carbon lattice. Our goal was to develop a code model of the NV center that can simulate its ODMR spectra, potentially accelerating the detection process.

# 2 Methods

This section systematically outlines our methodology and provides the necessary theoretical background for the model we employed. Our code is developed in Python and follows the steps mentioned in this section.

## 2.1 Single NV Hamiltonian

In its ground state, the negatively charged NV defect is a spin triplet $^3A_2$ as explained above. The degeneracy is lifted by a spin-spin interaction that decomposes the state into a single spin projection $m_s = 0$ and a doublet $m_s = \pm 1$ separated by $D_{gs} = 2.87$GHz at zero magnetic field bias. When a magnetic field $\vec{\boldsymbol{B}}$ is applied to the defect, it splits the doublet state further. In this scenario, the ground state Hamiltonian is written as follows:

$$\mathcal{H}_{gs} = hD_{gs}S_z^2 + \mu g\tilde{\mathbf{B}} \cdot \tilde{\mathbf{S}} \tag{1}$$

where only the zero-field splitting of the ground state and the Zeeman interaction with the static magnetic field are considered. Here, $h$ is Planck's constant, $\mu$ is the Bohr magneton, $g = 2.0028$ is Landé's g-factor, and $D_{\text{gs}} = 2.87\,\text{GHz}$ is the ground state splitting at zero magnetic field bias. We have neglected strain-induced splitting, temperature-induced splitting, and the effect of an electric field and the Stark effect. Additionally, the hyperfine interaction with nearby nuclear spins is neglected as well. While considering a single NV centre, the transverse field can be taken to lie along the x-axis. In the most general case, the Hamiltonian can be reduced to a 2-parameter model consisting of longitudinal and transverse magnetic terms [8]. Thus, the ground state Hamiltonian is :

$$\mathcal{H}_{gs} = hD_{gs}S_z^2 + \mu gB_zS_z + \mu gB_xS_x + \mu gB_yS_y \tag{2}$$

with $\mathcal{H}_{gs}^z = hD_{gs}S_z^2 + g\mu_B B_z S_z$ and $\mathcal{H}_{gs}^{\perp} = g\mu_B(B_xS_x + B_yS_y)$. The defect can be excited to a $^3E$ excited level by optical means. The $^3E$ level is also a spin triplet with zero-field splitting $D_{es} = 1.42$GHz with the same quantization axis and a similar gyromagnetic ratio as in the ground level [14]. Thus, the excited state Hamiltonian is given by Equation (1) while replacing $D_{gs}$ with $D_{es}$.

The eigenstates of the ground state are labelled $|1\rangle, |2\rangle, |3\rangle$ corresponding to the spin projections $m_s = 0$, -1 and +1. Similarly, the eigenstates of the excited states are labelled $|4\rangle, |5\rangle, |6\rangle$ corresponding to the spin projections $m_s = 0$, -1 and +1 [14].

Recent experiments have identified two singlet states, whereas theoretical studies predict the presence of a third singlet state. We have considered a single 'metastable' level labelled $|7\rangle$.

## 2.2 Seven-Level Model

We have adopted a simple seven-level model of the NV defect [14]. The ground state is a triplet that can be excited by 532nm wavelength laser light into the excited state triplet. The relaxation path followed subsequently will decide the amount of photons released.

The NV defect can relax through spin-conserving transitions, producing red PL. It can also relax through a secondary path involving the metastable state, producing no PL.

The 7 zero-field states $|i\rangle$ mentioned above form a complete basis. Applying a static magnetic field $\mathbf{B}$ results in the perturbation of these eigenstates. The perturbed eigenstates $|i\rangle^{'}$ can be represented as a linear combination of the original eigenstates $|i\rangle$ according to the following formula [14]:

$$|i\rangle^{'} = \sum_{j=1}^{7} \alpha_{ij}(\mathbf{B})\,|j\rangle \tag{3}$$

The $\alpha$ matrix's coefficients can be determined using Time Independent Perturbation Theory and are functions of the external static magnetic field applied [8].

Within this model, the zero field transition rates from $|i\rangle$ to $|j\rangle$ are denoted by $k_{ij}$. We consider that the optical transitions are purely spin-conserving and radiative relaxation is spin-independent. Thus, $k_{41} = k_{52} = k_{63} = k_r$ [14]. The optical pumping rates due to the applied green laser are proportional to the corresponding relaxation rates through $k_{ji} = \beta k_{ij}$ for $j = 1, 2, 3$ and $i = 4, 5, 6$, where $\beta$ is the optical pumping parameter. The inter-system crossing rates depend on the absolute value of $m_s$, i.e. $k_{57} = k_{67}$ and $k_{72} = k_{73}$ [2]. $\beta$ is a dimensionless parameter relating to the optical pumping rate as follows [10]:

$$\beta = \frac{\sigma}{k_r * h * \nu} * I \tag{4}$$

where $\sigma$ is the absorption cross-section of NV centres under 532 nm illumination, $\nu$ is the laser frequency, and $I$ is the intensity of the laser. The various transition rates are shown in Fig [1].
In a similar manner to the eigenstates, the transition rates will evolve as a combination of the zero-field transition rates as follows [14]:

$$k_{ij}^{'}(\mathbf{B}) = \sum_{p=1}^{7}\sum_{q=1}^{7} |\alpha_{ip}|^2 \, |\alpha_{jq}|^2 \, k_{pq} \tag{5}$$

The excitation due to the green laser causes the spin state populations to evolve with time. The populations can be calculated with the classical rate equation [14]:

$$\frac{dn_i}{dt} = \sum_{j=1}^{7}(k_{ji}n_j - k_{ij}n_i) \tag{6}$$

However, for the purposes of our experiment, the above equation will be solved in the state state condition i.e. $\frac{dn_i}{dt} \to 0$. This corresponds to an experimental setup where the NV centre has been excited long enough for all the transient behaviour to diminish. In other words, the rate of excitation from a particular state is equal to that state's relaxation rate. Our closed seven-level model uses the normalising condition $\sum_{i=1}^{7} = 1$. Thus, to calculate the steady-state spin state population $[\bar{n_i}]$, we solve the normalising condition along with the following set of equations:

$$0 = \sum_{j=1}^{7}(k_{ji}n_j - k_{ij}n_i) \tag{7}$$

The decay of the excited state to the ground state via the metastable state produces no PL. Thus, the total radiative decay or PL is only through the spin-conserving transitions. Thus, in the general case, the mean PL rate is given by [14]:

$$\bar{R}(\mathbf{B}) = \eta \sum_{i=4}^{6}\sum_{j=1}^{3} \bar{n_i} k_{ij} \tag{8}$$

where $\eta$ is the collection efficiency of the photon detector [8].

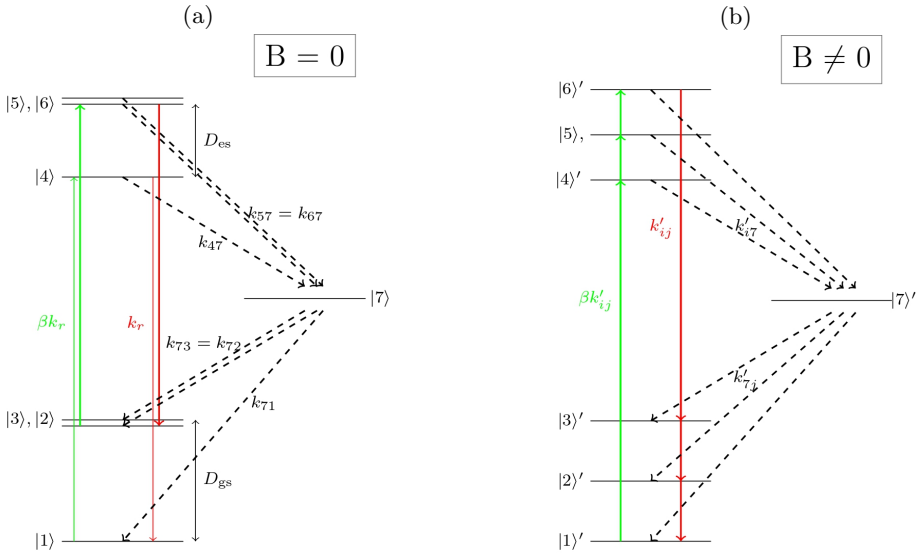


Figure 1: (a). Seven-level energy level structure considered for the NV defect at room temperature and zero static magnetic bias. The 5 intrinsic transitions $k_r, k_{47}, k_{57}, k_{71}, k_{72}$ are shown. (b). For an applied magnetic field B, all transition rates are likely to be non-zero due to electron spin mixing in both the excited and ground states.

## 2.3 Transition Rates due to Microwave

In Continuous-Wave ODMR, the spin transitions are probed by sweeping the applied MW over a range of frequencies. The microwave applied is of the form $\vec{B}_{MW}\cos(2\pi\omega t)$. We have coupled the effect of the MW field $\vec{B}_{MW}$ to the ground state Hamiltonian through the following interaction Hamiltonian:

$$H_{int} = \mu g B_z^{MW} S_z + \mu g B_x^{MW} S_x + \mu g B_y^{MW} S_y \tag{9}$$

The above interaction Hamiltonian induces transitions from $|1\rangle$ to $|2\rangle$ and from $|1\rangle$ to $|3\rangle$ and vice-versa. The microwave frequency at which these transitions happen is determined by the static magnetic field applied and the resulting difference between the energy levels due to the Zeeman Effect.
The transition rate between these states, denoted by $T_{12}$ and $T_{13}$ can be calculated using Time-Dependent Perturbation Theory and Fermi's Golden rule. The rate is calculated as:

$$T_{if} = \frac{2\pi}{\hbar} \left|\langle f| H_{int} |i\rangle\right|^2 \rho(E) \tag{10}$$

where $\rho(E)$ is the density function, a Lorentzian in our case. The Lorentzian is defined by an amplitude T and a linewidth $\delta_E$. The formula of the Lorentzian is as follows:

$$\rho(E) = \frac{\frac{\delta_E}{2}}{(E - E_f)^2 + (\frac{\delta_E}{2})^2} \tag{11}$$

where $E_f$ is the normalised eigenvalue of the final state with respect to the initial state. We convert the energy scale to the frequency scale by $\nu = \frac{E}{h}$. Thus, we can convert $\rho(E)$ to $\rho(\nu)$ by dividing by $h^2$ and using $\nu_f = \frac{E_f}{h}$ and using the frequency linewidth $\Delta\nu = \frac{\delta_E}{h}$. Thus:

$$\rho(\nu) = \frac{\frac{\Delta\nu}{2h}}{(\nu - \nu_f)^2 + (\frac{\Delta\nu}{2})^2} \tag{12}$$

The frequency-dependent transition rate between the initial and final state induced by the MW is thus:

$$T_{if}(v) = (\frac{2\pi}{\hbar}) \left|\langle f| H_{int} |i\rangle\right|^2 \rho(\nu) \tag{13}$$

## 2.4 Linewidth

The linewidth in the ODMR contrast graph first arises due to Heisenberg's Uncertainty Principle. At the transition frequency, the electron has a finite relaxation time from the excited to the ground state. This finite excitation time results in a finite $\Delta$E, which is the broadening of the graph at that point. Besides this natural broadening, there are two more reasons for a finite linewidth in the graph: power broadening due to the MW and the excitation laser [5].

At low microwave power, the transition between the spin states of the NV centre occurs at a specific resonance frequency, resulting in a sharp resonance peak. As the microwave power increases, the population of the spin states starts to saturate due to the increase in the rabi frequency. In other words, the rate of induced transitions between the states at resonance becomes comparable to the relaxation rates of those states. This saturation or population inversion causes the transitions to occur over a broader range of frequencies, leading to a broadening of the resonance peak.

As the power of the exciting green laser increases, the rate of optical excitation increases, leading to a higher population of NV centres in the excited state. This leads to a reduction of the cycle time. In other words, the relaxation and excitation cycle time is reduced, reducing the effective lifetime of the states. This reduction in uncertainty in T increases the uncertainty of E, increasing the linewidth.

The polarization rate $\Gamma_p$ is related to the rate of optical cycles and the effect of optical pumping. The optically induced polarization rate can be given by [5]:

$$\Gamma_p = \Gamma_p^\infty * \frac{s}{1+s} \tag{14}$$

where s = $\frac{P}{P_{sat}}$ is the ratio of the current laser power and the saturation power of the laser, after which the rate of transitions saturate [9], and $\Gamma_p^\infty \approx 5 * 10^6$Hz is the polarization rate at saturation. This quantity is fixed by the lifetime of the metastable state, which is approximately 200ns at room temperature [5]. The saturation power can be calculated using the formula [9]:

$$P_{sat} = \frac{\pi w_o^2}{2} * I_{sat} \tag{15}$$

where $w_o$ is the laser beam diameter and [9]:

$$I_{sat} = \frac{W_p^{sat} * c * h}{\sigma * \lambda} \tag{16}$$

where $c$ is the speed of light, $\lambda$ is the laser wavelength, $h$ is planck's constant, and $\sigma$ is the NV center cross section. $W_p^{sat}$ is the saturation excitation rate equal to $\beta^{sat} * k_r$. The value of $W_p^{sat} = 1.9 * 10^7$ Hz [9].

The relaxation rates of the spin states due to optical pumping can be written as [5]:

$$\Gamma_c = \Gamma_c^\infty * \frac{s}{1+s} \tag{17}$$

where $\Gamma_c$ is the relaxation rate $k_r$ defined earlier. The MW power is modelled using the Rabi frequency given by $\Omega_R = \mu g/h * B_{MW}$ where $B_{MW}$ is the absolute magnitude of the MW. The linewidth of the ESR Lorentzian is thus [5]:

$$\Delta\nu = \frac{\Gamma_c^\infty}{2\pi} * \sqrt{(\frac{s}{1+s})^2 + \frac{\Omega_R^2}{\Gamma_p^\infty \Gamma_c^\infty}} \tag{18}$$

## 2.5 ODMR Steps

There are 7 input parameters to our model - B,$\eta$, $P_{laz}, P_{MW}, \sigma, w$, initial k matrix.

| Parameter | Value |
|---|---|
| $P_{MW}$ | 5-50 dbm |
| $P_{Laz}$ | 0-1.2 Watt |
| $w_0$ | 18um |
| $\sigma$ | $9 \times 10^{-21} m^2$ |
| $\eta$ | 1 |

Table 1: The values of the parameters used in the simulation [9], [11].

The steps are followed in the code to plot the ODMR graph are summarised below and also shown in Appendix A and Fig [2].

1. **Eigenvalue and Eigenvector Calculation:** We use Equation (2) to calculate the ground and excited state eigenvalues and eigenvectors.

2. **Interaction Hamiltonian and Transition Strengths:** The interaction Hamiltonian is calculated using Equation (9). The frequency-dependent transition strengths $T_{12}$ and $T_{13}$ are then calculated using Equation (12). The linewidth for the Lorentzian is calculated using Equations (14, 15, 16, 17, 18). This results in an array of $T_{12}$ and $T_{13}$, which depend on frequency.

3. **Alpha Matrix Calculation:** The $\alpha$ matrix is calculated using Time-Independent perturbation theory. Over here $H_0 = hD_{gs}S_z^2 + \mu g B_z S_z$ and $\delta H = \mu g B_x S_x + \mu g B_y S_y$.

4. **New Rate Matrix:** The new rate matrix $k^{'}$ is calculated using equation (5). $\beta$ is calculated using Equation (4) and is used to calculate the excitation rates in the $k^{'}$ matrix. These updated rates are then used to compute the steady-state population values via Equation (7).

| Transition | Rate [MHz] |
|---|---|
| $k_r$ | 63.2 |
| $k_{47}$ | 10.8 |
| $k_{57}$ | 60.7 |
| $k_{71}$ | 0.8 |
| $k_{72}$ | 0.4 |

Table 2: The rate values used in the initial rate matrix. All transition rates not shown are taken to be 0 [6].

5. **Initial Photoluminescence (PL) Rate:** The initial PL rate is calculated using Equation (8).

6. **Frequency Sweep and Contrast Calculation:**

   - Once the Initial PL rate $C_0$ is calculated we use the frequency dependent transition rate to find the dip in PL at each frequency point.
   - After calculating the new rate matrix for the magnetic field applied as in step 4, we set $k_{12} = k_{21}$ to $T_{12}$ corresponding to the current frequency point. Similarly, $k_{13} = k_{31}$ is set to the corresponding value of $T_{13}$.
   - We now recalculate the population values using Equation (7). These values are using the calculate a new value of PL $C_f$ for the current frequency point
   - The contrast amplitude for the current frequency point is calculated as $C = \frac{C_0 - C_f}{C_0}$. This is repeated for all the frequency points in the MW sweep. This results in a contrast array which is plotted to show the ODMR.

# 3 From Single NV to NV Ensembles

In a diamond lattice, there are 4 possible crystallographic axes along which each of the 4 possible NV center align. The ground state Hamiltonian is defined in the NV reference frame, where the Z-axis is aligned with the NV axis. However, external applied fields are typically expressed in laboratory frame. For our case, we have considered the four NV axes represented by i=1,2,3,4 along the following direction vectors in the laboratory frame:

$$NV_1 = \left\{\sqrt{\frac{2}{3}}, 0, \sqrt{\frac{1}{3}}\right\}, NV_2 = \left\{0, -\sqrt{\frac{2}{3}}, -\sqrt{\frac{1}{3}}\right\}, NV_3 = \left\{0, \sqrt{\frac{2}{3}}, -\sqrt{\frac{1}{3}}\right\}, NV_4 = \left\{-\sqrt{\frac{2}{3}}, 0, \sqrt{\frac{1}{3}}\right\}$$

Furthermore, to solve for the NV ensemble, it is assumed that each NV orientation with two possible directions (NV, VN), has the same proportion in the diamond sample.This is generally true, however, a diamond with a preferential NV axis can be created by altering its growth conditions. Such cases can be implemented in our code by making the contributions to PL proportional to the proportion of orientations present.

The following steps can be used to extend our code from single to NV ensemble:

1. Transform the magnetic field (static, external, and microwave) along each NV frame. The transformation matrix for the lab frame to the NV frame, which depends on the direction vector of the NV axis defined in the lab frame, is given below:

$$RNV_1 = \begin{pmatrix} 0 & 1 & 0 \\ -\sqrt{\frac{1}{3}} & 0 & \sqrt{\frac{2}{3}} \\ \sqrt{\frac{2}{3}} & 0 & \sqrt{\frac{1}{3}} \end{pmatrix} \quad RNV_2 = \begin{pmatrix} 1 & 0 & 0 \\ 0 & \sqrt{\frac{1}{3}} & -\sqrt{\frac{2}{3}} \\ 0 & -\sqrt{\frac{2}{3}} & -\sqrt{\frac{1}{3}} \end{pmatrix}$$

$$RNV_3 = \begin{pmatrix} 1 & 0 & 0 \\ 0 & -\sqrt{\frac{1}{3}} & -\sqrt{\frac{2}{3}} \\ 0 & \sqrt{\frac{2}{3}} & -\sqrt{\frac{1}{3}} \end{pmatrix} \quad RNV_4 = \begin{pmatrix} 0 & 1 & 0 \\ \sqrt{\frac{1}{3}} & 0 & \sqrt{\frac{2}{3}} \\ -\sqrt{\frac{2}{3}} & 0 & \sqrt{\frac{1}{3}} \end{pmatrix}$$

2. To transform any vector from a NV to VN frame, change the sign of z-coordinate of vector in NV frame while the rest remains same.

3. Now, the same procedure can be followed as a single NV. We do that 8 times to calculate the photoluminescence $PL_{NV,i}$ and $PL_{VN,i}$ (for i=1,3,4 and 4) for all the possible orientations.

4. Total contrast for all 8 possible orientations can be defined by:

$$C_{ensemble}(\nu) = \frac{8C_0 - (\sum_{i=1}^{4} PL_{NV,i} + \sum_{i=1}^{4} PL_{VN,i})}{8C_0} \tag{19}$$

# 4 Results

The ODMR spectrum allows for the reconstruction of the magnetic field vector, which is fundamental to vector magnetometry. We follow the procedure outlined in Section 3 to process a list of external magnetic field values over a specified region, divided into discrete points with known magnetic fields at each point. Our code generates the ODMR spectrum for each magnetic field value in this list. In python, we speed this process up by using the Multiprocessing library, to compute multiple plots in parallel.Subsequently, we use these ODMR spectra to reconstruct the magnetic field at each point, thereby reconstructing the entire magnetic field vector in the region.

# References


[1] D. D. Awschalom, R. Hanson, J. Wrachtrup, and B. B. Zhou. Quantum technologies with optically interfaced solid-state spins. *Nature Photonics*, 12(9):516–527, 2018.

[2] A. Cooper, E. Magesan, H. N. Yum, and P. Cappellaro. Time-resolved magnetic sensing with electronic spins in diamond. *Nature Communications*, 5:3141, 2014.

[3] M. W. Doherty, N. B. Manson, P. Delaney, F. Jelezko, J. Wrachtrup, and L. C. Hollenberg. The nitrogen-vacancy colour centre in diamond. *Physics Reports*, 528(1):1–45, 2013.

[4] F. Dolde, H. Fedder, M. W. Doherty, T. Nöbauer, F. Rempp, G. Balasubramanian, T. Wolf, F. Reinhard, L. C. L. Hollenberg, F. Jelezko, and J. Wrachtrup. Electric-field sensing using single diamond spins. *Nature Physics*, 7(6):459–463, 2011.

[5] A. Dréau, M. Lesik, L. Rondin, P. Spinicelli, O. Arcizet, J-F. Roch, and V. Jacques. Avoiding power broadening in optically detected magnetic resonance of single nv defects for enhanced dc magnetic field sensitivity. *Physical Review B*, 84(19):195204, 2011.

[6] H. Duarte, H. T. Dinani, V. Jacques, and J. R. Maze. Effect of intersystem crossing rates and optical illumination on the polarization of nuclear spins close to nitrogen-vacancy centers. *Physical Review B*, 103(19):195443, 2021.

[7] J. S. Hodges, N. Y. Yao, D. Maclaurin, C. Rastogi, M. D. Lukin, and D. Englund. Timekeeping with electron spin states in diamond. *Physical Review A*, 87(3):032118, 2013.

[8] Nicolas A. Lopez. *All-optical method of nanoscale magnetometry for ensembles of nitrogen-vacancy defects in diamond*. PhD thesis, Massachusetts Institute of Technology, 2015.

[9] Simone Magaletti, Ludovic Mayer, Jean-François Roch, and Thierry Debuisschert. Modelling rabi oscillations for widefield radiofrequency imaging in nitrogen-vacancy centers in diamond. *New Journal of Physics*, 26(2):023020, 2024.

[10] Anand Patel, Zainab Chowdhry, Anil Prabhakar, A. Rathi, and V. P. Bhallamudi. Single and double quantum transitions in spin-mixed states under photo-excitation. *arXiv preprint*, arXiv:2306.17531, 2023.

[11] Charlie Oscar Oncebay Segura. *Diamond studies for applications in quantum technologies.* PhD thesis, Universidade de São Paulo, 2019.

[12] F. Shi et al. Single-protein spin resonance spectroscopy under ambient conditions. *Science*, 347(6226):1135–1138, 2015.

[13] V. V. Soshenko et al. Nuclear spin gyroscope based on the nv center in diamond. Sep 2020.

[14] Jean Philippe Tetienne, Loïc Rondin, Piernicola Spinicelli, Mayeul Chipaux, Thierry Debuisschert, Jean-François Roch, and Vincent Jacques. Magnetic-field-dependent photodynamics of single nv defects in diamond: an application to qualitative all-optical magnetic imaging. *New Journal of Physics*, 14(10):103033, 2012.

# 5 Appendix A. Algorithm

The steps followed in the code to calculate the ODMR spectra are summarised in the form of a flowchart algorithm.

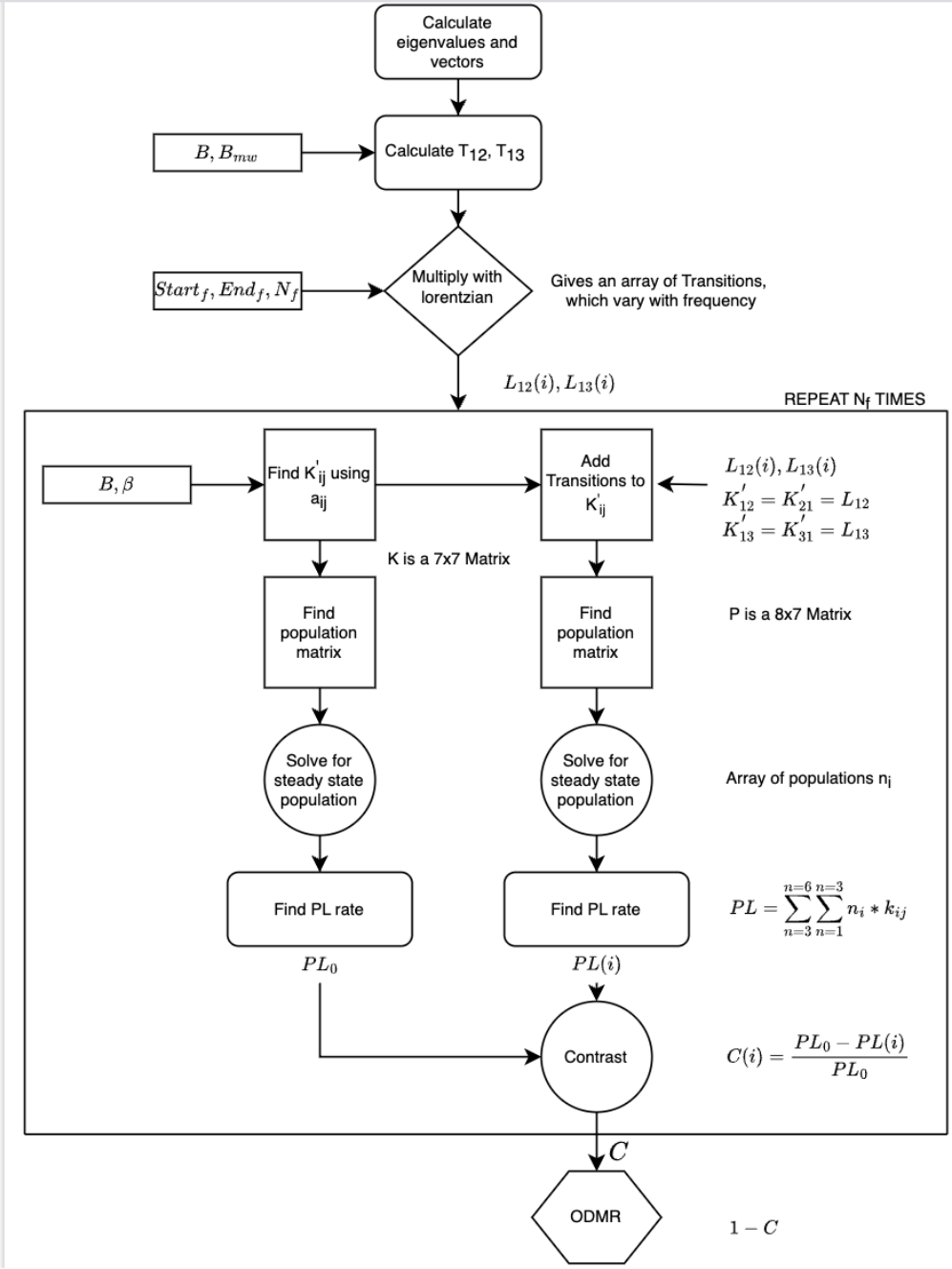


Figure 2: Algorithm followed in the code